



1 **Aerosol transport pathways and source attribution in China**
2 **during the COVID-19 outbreak**

3

4

5 Lili Ren¹, Yang Yang^{1*}, Hailong Wang², Pinya Wang¹, Lei Chen¹, Jia
6 Zhu¹, Hong Liao¹

7

8

9

10

11 ¹Jiangsu Key Laboratory of Atmospheric Environment Monitoring and Pollution
12 Control, Jiangsu Collaborative Innovation Center of Atmospheric Environment and
13 Equipment Technology, School of Environmental Science and Engineering, Nanjing
14 University of Information Science and Technology, Nanjing, Jiangsu, China

15 ²Atmospheric Sciences and Global Change Division, Pacific Northwest National
16 Laboratory, Richland, Washington, USA

17

18

19

20

21 *Correspondence to yang.yang@nuist.edu.cn

22



23 **Abstract**

24 Due to the coronavirus disease 2019 (COVID-19) pandemic, human
25 activities and industrial productions were strictly restricted during January-
26 March 2020 in China. Despite the fact that anthropogenic aerosol
27 emissions largely decreased, haze events still occurred. Characterization of
28 aerosol transport pathways and attribution of aerosol sources from specific
29 regions are beneficial to the air quality and pandemic control strategies.
30 This study establishes source-receptor relationships in various regions of
31 China during the COVID-19 outbreak based on the Community
32 Atmosphere Model version 5 with Explicit Aerosol Source Tagging
33 (CAM5-EAST). Our analysis shows that $PM_{2.5}$ burden over the North
34 China Plain between January 30 and February 19 is largely contributed by
35 local emissions (40–66%). For other regions in China, $PM_{2.5}$ burden is
36 largely contributed from non-local sources. During the polluted days of
37 COVID-19 outbreak, local emissions within North China Plain and Eastern
38 China, respectively, contribute 66% and 87% to the increase in surface
39 $PM_{2.5}$ concentrations. This is associated with the anomalous mid-
40 tropospheric high pressure at the location of climatological East Asia
41 trough and the consequently weakened winds in the lower troposphere,
42 leading to the local aerosol accumulation. The emissions outside China,
43 especially from South and Southeast Asia, contribute over 50% to the
44 increase in $PM_{2.5}$ concentration in Southwestern China through



45 transboundary transport during the polluted day. As the reduction in
46 emissions in the near future, aerosols from long-range transport together
47 with unfavorable meteorological conditions are increasingly important to
48 regional air quality and need to be taken into account in clean air plans.



49 **1. Introduction**

50 The coronavirus disease 2019 (COVID-19) had an outbreak in China
51 in December 2019. It has resulted in more than one million cases within
52 the first four months worldwide (Sharma et al., 2020; Dong et al., 2020).
53 In order to curb the virus spread among humans, China was the first
54 country to take dramatic measures to minimize the interaction among
55 people, including strict isolation, prohibition of large-scale private and
56 public gatherings, restriction of private and public transportation and even
57 lockdown of cities (Tian et al., 2020; Wang et al., 2020). The estimated
58 NO_x emission in eastern China was reduced by 60-70%, of which 70-80%
59 was related to the reduced road traffic and 20-25% was from industrial
60 enterprises shutdown during the COVID-19 lockdown period (Huang et al.,
61 2020). However, severe air pollution events still occurred in East China
62 during the COVID-19 lockdown. It is of great concern that why severe air
63 pollution was not avoided by decreasing anthropogenic emissions.

64 The unprecedented large-scale restrictions resulting from the COVID-
65 19 epidemic provide an opportunity to research the relationship between
66 dramatic anthropogenic emission reductions and air quality change (e.g.,
67 Bao et al., 2020; Li et al., 2020; Wang et al., 2020). Bao et al. (2020)
68 reported that, during the COVID-19 lockdown period, the air quality index
69 (AQI) and the PM_{2.5} (particulate matter less than 2.5 μm in diameter)
70 concentration were decreased by 7.8% and 5.9 %, respectively, on average



71 in 44 cities in northern China, mainly due to travel restrictions. By applying
72 the WRF-CAMx model together with air quality monitoring data, Li et al.
73 (2020) revealed that although primary particle emissions were reduced by
74 15%–61% during the COVID-19 lockdown over the Yangtze River Delta
75 Region, the daily mean concentration of $PM_{2.5}$ was still relatively high,
76 reaching up to $79 \mu\text{g m}^{-3}$. Wang et al. (2020) found that the relative
77 reduction in $PM_{2.5}$ precursors was twice as much as the reduction in $PM_{2.5}$
78 concentration, in part due to the unfavorable meteorological conditions
79 during the COVID-19 outbreak in China that led to the formation of the
80 heavy haze. Huang et al. (2020) and Le et al. (2020) reported that stagnant
81 air conditions, high atmospheric humidity, and enhanced atmospheric
82 oxidizing capacity led to a severe haze event in northern China during the
83 COVID-19 pandemic.

84 Aerosols are main air pollutants that play important roles in the
85 atmosphere due to their adverse effects on air quality, visibility (Vautard et
86 al., 2009; Watson, 2002), human health (Lelieveld et al., 2019; Heft-Neal
87 et al., 2018), the Earth's energy balance, and regional and global climate
88 (Ramanathan et al., 2001; Anderson et al., 2003; Wang et al., 2020; Smith
89 et al., 2020). With the rapid development in recent decades, China has
90 experienced severe air pollutions that damage human health and cause
91 regional climate change (Chai et al., 2014; Liao et al., 2015; Fan et al.,
92 2020). In order to control air pollution, the Chinese government issued and



93 implemented the Air Pollution Prevention and Control Action Plan in 2013
94 (China State Council, 2013). Although emissions in China have decreased
95 significantly in recent years (Zheng et al., 2018), aerosols transported from
96 other source regions could add on top of local emissions (Yang et al., 2017a,
97 2018a; Ren et al., 2020). Therefore, it is important to understand the
98 relative effects of local emissions and regional transport on aerosols in
99 China.

100 Source tagging and apportionment is an effective way to establish
101 aerosol source-receptor relationships, which is conducive to both scientific
102 research and emission control strategies (Yu et al., 2012). By applying the
103 Particulate Source Apportionment Technology in CAMx model, Xue et al.
104 (2014) found that the contributions of regional transport to annual average
105 $PM_{2.5}$ concentrations in Hainan, Shanghai, Jiangsu, Zhejiang, Jilin and
106 Jiangxi provinces of China are more than 45%. By adding a chemical tracer
107 into the WRF model, Wang et al. (2016) studied the sources of black carbon
108 (BC) aerosol in Beijing and reported that about half of BC in Beijing came
109 from the central North China Plain. Liu et al. (2017) applied WRF-Chem
110 model and showed that Foshan, Guangzhou and Dongguan, respectively,
111 with relatively high emissions contributed 14%, 13% and 10% to the
112 regional mean $PM_{2.5}$ concentration in the Pearl River Delta.

113 Currently, many studies have investigated the impact of reduced human
114 activity on regional air quality, as a result of the COVID-19 outbreak. Few



115 studies have focused on aerosol transport pathways and source attribution
116 in China during the COVID-19 pandemic. In this study, the global aerosol-
117 climate model CAM5 (Community Atmosphere Model, version 5)
118 equipped with an Explicit Aerosol Source Tagging (CAM5-EAST) is
119 employed to quantify source-receptor relationships and transport pathways
120 of aerosols during the COVID-19 outbreak in China. We also provide
121 model evaluations of PM_{2.5} concentrations against observations made
122 during the COVID-19 outbreak. With the aerosol source tagging technique,
123 source region contributions to PM_{2.5} column burden over various receptor
124 regions and transport pathways in China are analyzed. The source
125 contributions to the changes in near-surface PM_{2.5} in polluted days
126 compared to the monthly means during February 2020 are also quantified.
127 This paper provides source apportionment of aerosols in China during the
128 COVID-19 emission reductions, which is beneficial to the investigation of
129 policy implications for future air pollution control.

130 **2. Methods**

131 **2.1 Model description and experimental setup**

132 The CAM5 model is applied to estimate the PM_{2.5} changes during the
133 COVID-19 period. In CAM5, which is the atmospheric component of the
134 earth system model CESM (Community Earth System Model, Hurrell et
135 al., 2013). In this study, major aerosol species including sulfate, BC,
136 primary organic matter (POM), secondary organic aerosol (SOA), sea salt,



137 and mineral dust, are represented by three lognormal size modes (i.e.,
138 Aitken, accumulation, and coarse modes) of the modal aerosol module
139 (MAM3) (Liu et al., 2012). The detailed aerosol representation in CAM5
140 was provided in Liu et al. (2012) and Wang et al. (2013). The aerosol
141 mixing states consider both internal mixed (within a same mode) and
142 external mixed (between modes). On top of the default CAM5, additional
143 modifications that improve the representation of aerosol wet scavenging
144 and convective transport (Wang et al., 2013) are also included in the model
145 version used for this study.

146 In this study, simulations were conducted with a horizontal resolution
147 of $1.9^\circ \times 2.5^\circ$ and 30 vertical layers up to 3.6 hPa in year 2020.
148 Anthropogenic emissions in China are derived from the MEIC (Multi-
149 resolution Emission Inventory of China) inventory (Zheng et al., 2018).
150 while emissions for the other countries use the SSP (Shared Socioeconomic
151 Pathways) 2–4.5 scenario data set under CMIP6 (the Coupled Model
152 Intercomparison Project Phase 6). Emissions in year 2017 are used as the
153 baseline during the simulation period considering the time limit of MEIC
154 inventory. To better estimate the impact of restricted human activities on
155 emission reductions owing to COVID-19 lockdown, we updated China's
156 emission inventory from January to March 2020 based on the provincial
157 total emission reduction ratio in Huang et al. (2020). Emissions from the
158 transportation sector are decreased by 70% and the remaining reductions



159 are evenly distributed to other sectors from January to March 2020
160 compared to the baseline emission in 2017. The sea surface temperature,
161 sea ice concentrations, solar radiation and greenhouse gas concentrations
162 are fixed at present-day climatological levels. To capture the large-scale
163 atmospheric circulations during the COVID-19, we nudge the model wind
164 fields toward the MERRA-2 (Modern-Era Retrospective Analysis for
165 Research and Applications, version 2) reanalysis (Gelaro et al., 2017) from
166 April 2019 to March 2020 repeatedly for six years. Only model results from
167 the last year are used to represent year 2020. In this study, we analyze the
168 transport pathways and source attribution of aerosols during the three
169 weeks that had the largest number of newly-diagnosed COVID-19 cases
170 (Fig. 2, hereafter referred to as the ‘Week 1’: January 30–February 5,
171 ‘Week 2’: February 6–February 12 and ‘Week 3’: February 13–February
172 19), when unexpected hazardous air pollution events also occurred during
173 this time period (Le et al., 2020).

174 **2.2 Explicit aerosol source tagging and source regions**

175 To examine the source apportionment of aerosols in China, the Explicit
176 Aerosol Source Tagging (EAST) technique was implemented in CAM5,
177 which has been utilized in many aerosol source attribution studies (e.g.,
178 Wang et al., 2014; Yang et al., 2017a, b, 2018a, b, c, 2020; Ren et al., 2020).
179 Different from the emission sensitivity method that assumes a linear
180 response to emission perturbation and the traditional backward trajectory



181 method, aerosols from each tagged region or sector are calculated
182 independently in EAST within one single simulation. Without relying on a
183 set of model simulations with emission perturbations or assuming constant
184 decaying rate, EAST is more accurate and time-saving than the source
185 apportionment method mentioned above. In addition to the sulfate, BC and
186 POM species that were tagged in previous studies (e.g., Yang et al., 2020),
187 SOA and precursor gas are now also tagged in the EAST. These types of
188 aerosols from independent source regions and sectors can be explicitly
189 tagged and tracked simultaneously. In this study, focusing on the aerosols
190 in China during the COVID-19 outbreak period, the domestic aerosol and
191 precursor emissions are divided into eight geographical source regions (Fig.
192 1), including Northeastern China (NEC), North China Plain (NCP), Eastern
193 China (ESC), Southern China (STC), Central-West China (CWC),
194 Southwestern China (SWC), Northwestern China (NWC) and the
195 Himalayas and Tibetan Plateau (HTP), and the rest of the world (ROW)
196 emissions are tagged separately.

197 **3. Model evaluation**

198 Many previous studies have assessed the spatial distribution and
199 seasonal to decadal variations in aerosol concentrations in China and
200 worldwide simulated by CAM5 with the observations (e.g., Wang et al.,
201 2013; Yang et al., 2017a,b, 2018b,c, 2020). In order to evaluate the model's
202 performance in simulating aerosols during the COVID-19 outbreak period



203 in China, the surface concentrations of $PM_{2.5}$, estimated as the sum of
204 sulfate, BC, POM and SOA for model results, during the analyzed time
205 periods are compared with measurements from the China National
206 Environmental Monitoring Center (CNEMC), as shown in Fig. 3a. The
207 model reasonably reproduces the overall spatial distribution of near-
208 surface $PM_{2.5}$ concentrations during the three time periods, with high
209 values in the North China Plain and low values in western China. However,
210 as reported in many CAM5 model studies (e.g., Yang et al., 2017a,b), the
211 model underestimates the $PM_{2.5}$ concentrations with normalized mean
212 biases (NMB) of -55%~-49%, compared to the available site observations
213 (Fig. S1). The discrepancies are related to coarse-resolution model
214 sampling bias relative to the observational sites, uncertainties in aerosol
215 emissions, wet removal, and gas-particle exchange. In addition, the model
216 version used in this study is not able to simulate nitrate and ammonium
217 aerosols, which are also the main components of $PM_{2.5}$ (Kong et al., 2020;
218 Xu et al., 2019).

219 The long-distance transport of aerosols mainly occurs in the upper
220 troposphere rather than near the surface (Hadley et al., 2007; Zhang et al.,
221 2015). Aerosols are lifted from the atmospheric boundary layer of the
222 emission source regions to the free troposphere and then undergo the
223 transboundary and intercontinental transport effectively driven by the
224 upper tropospheric circulations. Therefore, it is helpful to analyze the



225 relative contributions of local and non-local sources by focusing on the
226 column burden of aerosols. Figure 3b presents spatial distributions of
227 simulated mean column burden of $\text{PM}_{2.5}$ during the three time periods. The
228 contrast in column burden does not differ significantly from that of near-
229 surface concentrations. Among the three time periods, Week 1 and Week 2
230 have higher $\text{PM}_{2.5}$ loading, with values in the range of 20–40 and 20–30
231 mg m^{-2} in the North China Plain, Eastern China, and Southern China, while
232 the $\text{PM}_{2.5}$ loading in Week 3 is relative lower with values ranging mostly
233 from 10 to 20 mg m^{-2} . Note that the column burden of $\text{PM}_{2.5}$ in South and
234 Southeast Asia is higher than 20 mg m^{-2} in three time periods and reaches
235 up to 50 mg m^{-2} in Week 2, which potentially influences aerosol
236 concentrations in China through transboundary transport.

237 **4. Transport Pathways**

238 The explicit aerosol tagging technique can clearly identify the transport
239 pathways of aerosols moving from their source regions to their destination.
240 Figure 4 shows the spatial distribution of mean column burden of simulated
241 $\text{PM}_{2.5}$ originating from the six tagged source regions in central and eastern
242 China and outside of China during the three time periods. Aerosols and/or
243 precursor gases emitted from the various regions follow quite different
244 transport pathways determined by their source locations, meteorological
245 conditions, emission injection height, and physical and chemical
246 characteristics of aerosol species. Aerosols from Northeastern China are



247 transported southeastward by the northwesterly winds (Fig. 1b). From the
248 North China Plain, aerosols can be transported either southward reaching
249 Eastern, Southern and Southwestern China during Week 1 or across east
250 coast of China to the oceanic region during Week 2-3. Aerosols originating
251 from Eastern China move straight to Southwestern and Southern China
252 during Week 1-2, while they also entered the North China Plain during
253 Week 2-3. Aerosols emitted from Southern China and Central-West China
254 have no obvious transport due to their relatively weak emissions. In
255 additional to the local impact, emissions from Southwestern China affect
256 mostly the Southern China and Eastern China. Air parcels with high levels
257 of $PM_{2.5}$ from South and Southeast Asia moved into Southwestern,
258 Southern and Eastern China and even the North China Plain during the
259 three time periods.

260 The vertical distributions of $PM_{2.5}$ emitted from six major tagged
261 source regions are shown in Figs. S2 and S3. The $PM_{2.5}$ has much higher
262 concentrations in the lower troposphere and decreases with increasing
263 height. During Week 1-2, owing to the presence of high $PM_{2.5}$ loadings, a
264 stronger vertical mixing and transport brought more $PM_{2.5}$ to the upper
265 troposphere compared to that during Week 3. High concentrations of $PM_{2.5}$
266 originating from the North China Plain extended southeastward by strong
267 northwesterly winds. Weak winds over Eastern China led to accumulations
268 of $PM_{2.5}$ within this region, which is consistent with the findings in Yang



269 et al. (2017a). Strong southwesterly winds in the south of Southwestern
270 China and weak winds in the north of this region produced convergences
271 and updrafts that lift aerosols up to 700 hPa.

272 Considering that the emissions outside China contribute greatly to
273 $PM_{2.5}$ concentrations in Southwestern China through transboundary
274 transport (Yang et al., 2017a) and aerosols from East Asia can be
275 transported to the North Pacific and even North America (Yu et al., 2008;
276 Yang et al., 2018c), it is of great importance to study the inflow and outflow
277 of $PM_{2.5}$ across the boundaries of China. Figures 5 and 6 show the vertical
278 distribution of $PM_{2.5}$ concentrations resulting from emissions within and
279 outside China over $29^{\circ}N$, $88^{\circ}E$ and $21^{\circ}N$ around the south boundaries
280 (cross-sections (CS) 1-3 in Fig. 1a) and $123^{\circ}E$ around the east boundary
281 (CS 4 in Fig. 1a) of the mainland of China. Over the southern border, $PM_{2.5}$
282 concentrations are more influenced by transboundary transport of aerosols
283 from ROW than those originating from domestic emissions. The high
284 concentrations of $PM_{2.5}$ from South and Southeast Asia are lifted into the
285 free atmosphere of the Tibetan Plateau and Yun-Gui Plateau, and then
286 transported to Southern and Southwestern China by southwesterly winds.
287 Over the North China Plain and Eastern China, northwesterly winds at 35-
288 $45^{\circ}N$ and southwesterly winds at $25-35^{\circ}N$ cause aerosols to accumulate
289 in the lower atmosphere and then export across east border of China below
290 700 hPa.



291 **5. Source apportionment of PM_{2.5} in China during the COVID-19**

292 **5.1 Source contributions to PM_{2.5} burden**

293 Figure 7 shows the simulated relative contributions in percentage to
294 PM_{2.5} column burden from local source emissions, regional transport from
295 the untagged regions of China (rest of China, RCN) and rest of the world
296 (ROW). Over the North China Plain, where emissions are relatively high,
297 PM_{2.5} column burden is dominated by local emissions during the three time
298 periods. In contrast, regions with relative low emissions are mainly
299 affected by nonlocal sources, especially by foreign contributions.
300 Emissions from the ROW contribute a large amount to PM_{2.5} burden over
301 Northeastern, Southern, Central-West, Southwestern, Northwestern China
302 and the Tibetan Plateau. PM_{2.5} burden in Eastern China is greatly
303 contributed by the sources from RCN, especially in Week 1 when regional
304 transport of PM_{2.5} from the North China Plain is relatively strong (Fig. S3).

305 Table 1 summarizes the contributions of tagged source regions to the
306 PM_{2.5} burden over different receptor regions in China. In Northeastern
307 China, 36%-43% of the PM_{2.5} column burden comes from local emissions,
308 while a larger portion (39%-54%) is contributed by emissions from ROW
309 during the three time periods. The impacts of nonlocal sources within
310 China on PM_{2.5} burden are relatively low in Northeastern China during
311 Week 1 with the contribution of less than 5%, while RCN is responsible for
312 23% and 25% during Week 2 and Week 3, respectively.



313 In the North China Plain, the majority of the $PM_{2.5}$ burden is attributed
314 to local emissions in all cases, with local contributions in a range of 40–
315 66%. Emissions from the North China Plain also produce a widespread
316 impact on $PM_{2.5}$ over its neighboring regions. The sources from North
317 China Plain account for 14–33% of the $PM_{2.5}$ burden in Eastern China and
318 7–23% in Southern China during the three time periods.

319 In Eastern China, local emissions account for 27–40% of $PM_{2.5}$ column
320 burden, while ROW contributes 20–45%. Southern China and Central-
321 West China have 13–18% and 25–31% of local source contributions,
322 respectively, whereas 37–64% are due to emissions from outside China in
323 these two regions. In Southwestern China, 15–18% of the $PM_{2.5}$ burden
324 originates from local emissions and 7–24% is from RCN. ROW emissions
325 play important roles in affecting $PM_{2.5}$ burden over this region, with
326 relative contributions in a range of 59–78% during the three time periods,
327 which is associated with the transboundary transport by southwesterly
328 winds. $PM_{2.5}$ burden over the Northwestern China and Himalayas and
329 Tibetan Plateau with relatively low local emissions are strongly influenced
330 by nonlocal sources, where more than 70% of the $PM_{2.5}$ burden originates
331 from emissions outside China.

332 **5.2 Aerosol source attribution during polluted days**

333 In spite of the large reductions in emissions, severe air pollution events
334 still occurred in China during the COVID-19 lockdown. Source attribution



335 of $PM_{2.5}$ during polluted days in China has policy implications for future
336 air pollution control. In Beijing, capital of China over the North China
337 Plain, a serious haze event happened from February 11 to 13, 2020 during
338 the COVID-19 outbreak period according to observations released by
339 CNEMC. CAM5-EAST reproduced the polluted day on February 11 over
340 the North China Plain. In this study, the most polluted day is defined as the
341 day with the highest daily $PM_{2.5}$ concentration in February 2020 for each
342 receptor region in China. Figure 8 presents the composite differences in
343 near-surface $PM_{2.5}$ concentrations and 850 hPa wind fields between
344 polluted days and normal days (all days in February 2020) for each receptor
345 region. The local and nonlocal source contributions to the $PM_{2.5}$ differences
346 are summarized in Fig. 9.

347 Unexpectedly, near-surface $PM_{2.5}$ concentrations in the North China
348 Plain and Eastern China experienced remarkable increases during the
349 polluted days of COVID-19 lockdown. The simulated $PM_{2.5}$ concentrations
350 increased, with the largest increases of more than $20 \mu\text{g m}^{-3}$ in the North
351 China Plain and Eastern China, $10 \mu\text{g m}^{-3}$ maximum increase in the
352 Southwestern China and $5 \mu\text{g m}^{-3}$ in the Northeastern, Southern and
353 Central-West China, during the most polluted days compared to the normal
354 days.

355 The increase in near-surface $PM_{2.5}$ concentrations during the most
356 polluted day over Northeastern China is largely influenced by the local



357 emissions, which contribute to a regional averaged concentration increase
358 of $1.1 \mu\text{g m}^{-3}$. This is mainly due to the accumulation of local aerosols
359 under the weakened prevailing northwesterly winds over this region.

360 When the $\text{PM}_{2.5}$ pollution occurred in the North China Plain, the
361 concentration of $\text{PM}_{2.5}$ was $16.1 \mu\text{g m}^{-3}$ higher than that in normal days.
362 The contribution from local emissions accounts for 66% of the averaged
363 increase, which was related to the stagnant air condition (i.e., weakened
364 lower tropospheric winds) resulting from the anomalous mid-tropospheric
365 high pressure located at the climatological location of the East Asia trough
366 (Fig. S4). Sources from Eastern China also explain $4.3 \mu\text{g m}^{-3}$ (27%) of the
367 total increase over the North China Plain.

368 During the most polluted day in Eastern China (the same day as the
369 polluted day in North China Plain), the regional averaged increase in $\text{PM}_{2.5}$
370 concentrations is $16 \mu\text{g m}^{-3}$, which is primarily contributed by the local
371 emissions. While the contribution from the North China Plain decreased in
372 the polluted day, the anomalous southerly winds brought more aerosols
373 from Southern China and ROW into Eastern China, contributing to 4% and
374 10% aerosol increase, respectively.

375 Owing to the enhanced northerly winds, emissions from the North
376 China Plain and Eastern China contribute 33% and 39% of the increase,
377 respectively, in $\text{PM}_{2.5}$ concentration over Southern China. The most
378 polluted day in Central-West China is mostly caused by local emissions



379 (65% of the total increase).

380 When Southwestern China was under the polluted condition, PM_{2.5}
381 concentration was increased by 2.1 µg m⁻³. Emissions from ROW,
382 especially those from South and Southeast Asia, are of great significance
383 to the increase of PM_{2.5} concentrations due to the enhanced southwesterly
384 winds over this region. The relative contribution from ROW emissions is
385 more than 50% over Southwestern China during the most polluted day. It
386 highlights that the important role of transboundary transport needs to be
387 considered when controlling local emissions to improve air quality in the
388 near future.

389

390 **6. Conclusions and discussions**

391 An explicit aerosol source tagging is implemented in the Community
392 Atmosphere Model version 5 (CAM5-EAST) to examine the aerosol
393 transport pathways and source attribution of PM_{2.5} in China during the first
394 few weeks of the COVID-19 outbreak (Week 1: January 30–February 5,
395 Week 2: February 6–February 12 and Week 3: February 13–February 19).
396 The contributions of emissions to PM_{2.5} originating from eight source
397 regions in the mainland of China, including Northeastern China, North
398 China Plain, Eastern China, Southern China, Central-West China,
399 Southwestern China, Northwestern China and Himalayas and Tibetan
400 Plateau, and sources outside China (ROW) to near-surface concentrations,



401 column burdens, transport pathways of $PM_{2.5}$, and haze formation in
402 different receptor regions in China are quantified in this study.

403 Aerosols emitted from the North China Plain, where the air quality is
404 often poor, can be transported through Eastern China and reach
405 Southwestern China during the three time periods. Similarly, aerosols from
406 Eastern China move straight to Southern China and Southwestern China
407 during Week 1 and Week 2, and a significant portion can also enter the
408 North China Plain during Week 2 and Week 3.

409 Across the southern boundary of the mainland of China, high
410 concentrations of $PM_{2.5}$ from South and Southeast Asia are lifted into the
411 free atmosphere and then transported to Southern and Southwestern China.
412 While $PM_{2.5}$ from the North China Plain and Eastern China can also be
413 brought out of China via westerly winds, mostly below 700 hPa.

414 $PM_{2.5}$ in China is affected not only by local emissions but also by long-
415 range transport of pollutants from distant source regions. Over the North
416 China Plain, 40–66% of the $PM_{2.5}$ burden is attributed to local emissions
417 during the COVID-19 outbreak. They also impact $PM_{2.5}$ in neighboring
418 regions, accounting for 14–33% of the $PM_{2.5}$ burden in Eastern China and
419 7–23% in Southern China during the three time periods. Northeastern
420 China has 36%–43% of local source contributions to its $PM_{2.5}$ column
421 burden, while 39%–54% is contributed by emissions from ROW during the
422 three time periods. In Eastern China, local emissions explain 27–40% of



423 PM_{2.5} burden, while ROW contributes 20–45%. In Southwestern China,
424 59–78% of the PM_{2.5} burden is contributed by emissions from ROW. Over
425 the Northwestern China and Himalayas and Tibetan Plateau, ROW
426 emissions have a great contribution of more than 70% to the PM_{2.5} column
427 burden.

428 Despite the large reductions in emissions, near-surface PM_{2.5}
429 concentrations in the North China Plain and Eastern China increased a lot
430 during the most polluted days of COVID-19 lockdown (with the highest
431 daily PM_{2.5} concentration in February 2020), with the largest increases of
432 more than 20 µg m⁻³. In addition to local emissions, regional transport of
433 pollutants is also an important factor that causes haze events in China. The
434 increases in PM_{2.5} concentrations during the most polluted days over the
435 North China Plain and Eastern China are largely influenced by the stagnant
436 air condition resulting from the anomalous high pressure system and
437 weakening of winds, which lead to a reduced ventilation and aerosol
438 accumulation in the North China Plain, together with an increase in aerosol
439 inflow from regional transport. During the most polluted day in
440 Southwestern China, ROW contributes over 50% of the PM_{2.5}
441 concentration increase, with enhanced southwesterly winds that drive
442 pollution transport from South and Southeast Asia. It indicates that regional
443 transport and unfavorable meteorology need to be taken into consideration
444 when controlling local emissions to improve air quality in the near future.



445 There are a few uncertainties in this study. The CAM5 model has low
446 biases in reproducing the near-surface $\text{PM}_{2.5}$ concentrations in China,
447 compared to observations, in part due to the incapability of simulating
448 some aerosol components of $\text{PM}_{2.5}$ (e.g., ammonium and nitrate), excessive
449 aerosol wet removal during the long-range transport (Wang et al., 2013),
450 and uncertainties in observations. Uncertainties in the estimate of emission
451 reductions in different source regions during the COVID-19 pandemic can
452 also introduce uncertainties to our results. During the COVID-19 lockdown,
453 greenhouse gas emissions also decreased (Le Quéré et al., 2020), but the
454 effect of greenhouse gas reduction on meteorology that potentially
455 influence aerosol distributions was not taken into consideration.
456 Nevertheless, this study is the first attempt to provide source
457 apportionment of aerosols in China during the COVID-19 outbreak, which
458 is beneficial to the investigation of policy implications for future air
459 pollution control.



460 ***Data availability.***

461 The CAM5 model is available at
462 <http://www.cesm.ucar.edu/models/cesm1.2/> (last access: 25 October 2020).
463 CAM5-EAST model code and results can be made available upon request.
464 The surface PM_{2.5} observations are from the China National Environmental
465 Monitoring Center (CNEMC, <http://www.cnemc.cn>, last access: 25
466 October 2020)

467 ***Competing interests.***

468 The authors declare that they have no conflict of interest.

469 ***Author contribution.***

470 YY and LR designed the research; YY performed the model simulations;
471 LR analyzed the data. All authors discussed the results and wrote the paper.

472 ***Acknowledgments.***

473 This study was supported by the National Key Research and Development
474 Program of China (grant 2020YFA0607803) and the National Natural
475 Science Foundation of China (grant 41975159). HW acknowledges the
476 support by the U.S. Department of Energy (DOE), Office of Science,
477 Office of Biological and Environmental Research (BER). The Pacific
478 Northwest National Laboratory (PNNL) is operated for DOE by the
479 Battelle Memorial Institute under contract DE-AC05-76RLO1830.



480 Reference

481

482 Anderson, T.L., Charlson, R.J., Schwartz, S.E., Knutti, R., Boucher, O., Rodhe, H., Heintzenberg,
483 J.: Climate forcing by aerosol—a hazy picture, *Science*, 300, 1103-1104,
484 <https://doi.org/10.1126/science.1084777>, 2003.

485

486 Bao, R., Zhang, A.: Does lockdown reduce air pollution? Evidence from 44 cities in northern China,
487 *Science of The Total Environment*, 731, 139052,
488 <https://doi.org/10.1016/j.scitotenv.2020.139052>, 2020.

489

490 Chai, F., Gao, J., Chen, Z., Wang, S., Zhang, Y., Zhang, J., Zhang, H., Yun, Y., Ren, C.: Spatial and
491 temporal variation of particulate matter and gaseous pollutants in 26 cities in China, *Journal of*
492 *Environmental Sciences*, 26, 75–82, [https://doi.org/10.1016/S1001-0742\(13\)60383-6](https://doi.org/10.1016/S1001-0742(13)60383-6), 2014.

493

494 China State Council: Action Plan on Prevention and Control of Air Pollution, China State Council,
495 Beijing, China, http://www.gov.cn/zwggk/2013-09/12/content_2486773.htm (last access: 27
496 September 2020), 2013.

497

498 Dong, E., Du, H., Gardner, L.: An interactive web-based dashboard to track COVID-19 in real time,
499 *Lancet Infectious Diseases*, 20, 533–534, [https://doi.org/10.1016/S1473-3099\(20\)30120-1](https://doi.org/10.1016/S1473-3099(20)30120-1),
500 2020.

501

502 Fan, H., Zhao, C., Yang, Y.: A comprehensive analysis of the spatio-temporal variation of urban air
503 pollution in China during 2014–2018, *Atmospheric Environment*, 220, 117066,
504 <https://doi.org/10.1016/j.atmosenv.2019.117066>, 2020.

505

506 Gelaro, R., McCarty, W., Suárez, M. J., Todling, R., Molod, A., Takacs, L., Randles, C. A.,
507 Darmenov, A., Bosilovich, M. G., Reichle, R., Wargan, K., Coy, L., Cullather, R., Draper, C.,
508 Akella, S., Buchard, V., Conaty, A., da Silva, A. M., Gu, W., Kim, G., Koster, R., Lucchesi, R.,
509 Merkova, D., Nielsen, J. E., Partyka, G., Pawson, S., Putman, W., Rienecker, M., Schubert, S.
510 D., Sienkiewicz, M., Zhao, B.: The Modern-Era Retrospective Analysis for Research and
511 Applications, Version 2 (MERRA-2), *J. Climate*, 30, 5419–5454, [https://doi.org/10.1175/JCLI-](https://doi.org/10.1175/JCLI-D-16-0758.1)
512 [D-16-0758.1](https://doi.org/10.1175/JCLI-D-16-0758.1), 2017.

513

514 Hadley, O. L., Ramanathan, V., Carmichael, G. R., Tang, Y., Corrigan, C. E., Roberts, G. C., Mauger,
515 G. S.: Trans-Pacific transport of black carbon and fine aerosol ($D < 2.5\mu\text{m}$) into North America,
516 *Journal of Geophysical Research*, 112, D05309, <https://doi.org/10.1029/2006JD007632>, 2007.

517

518 Heft-Neal, S., Burney, J., Bendavid, E., Burke, M.: Robust relationship between air quality and
519 infant mortality in Africa, *Nature*, 559, 254. <https://doi.org/10.1038/s41586-018-0263-3>, 2018.

520

521 Hurrell, J. W., Holland, M. M., Gent, P. R., Ghan, S., Kay, J. E., Kushner, P. J., Lamarque, J. F.,
522 Large, W. G., Lawrence, D., Lindsay, K., Lipscomb, W. H., Long, M. C., Mahowald, N.,



- 523 Marsh, D. R., Neale, R. B., Rasch, P., Vavrus, S., Vertenstein, M., Bader, D., Collins, W. D.,
524 Hack, J. J., Kiehl, J., Marshall, S.: The Community Earth System Model A Framework for
525 Collaborative Research, *Bulletin Of The American Meteorological Society*, 94, 1339–1360,
526 <https://doi.org/10.1175/BAMS-D-12-00121.1>, 2013.
527
- 528 Huang, X., Ding, A., Gao, J., Zheng, B., Zhou, D., Qi, X., Tang, R., Ren, C., Nie, W., Chi, X., Wang,
529 J., Xu, Z., Chen, L., Li, Y., Che, F., Pang, N., Wang, H., Tong, D., Qin, W., Cheng, W., Liu, W.,
530 Fu, Q., Chai, F., Davis, S. J., Zhang, Q., He, K.: Enhanced secondary pollution offset reduction
531 of primary emissions during COVID-19 lockdown in China, *National Science Review*,
532 nwaal37, <https://doi.org/10.1093/nsr/nwaa137>, 2020.
533
- 534 Kong, L., Feng, M., Liu, Y., Zhang, Y., Zhang, C., Li, C., Qu, Y., An, J., Liu, X., Tan, Q., Cheng, N.,
535 Deng, Y., Zhai, R., Wang, Z.: Elucidating the pollution characteristics of nitrate, sulfate and
536 ammonium in PM_{2.5} in Chengdu, southwest China, based on 3-year measurements,
537 *Atmospheric Chemistry and Physics*, 20, 11181–11199, [https://doi.org/10.5194/acp-20-11181-](https://doi.org/10.5194/acp-20-11181-2020)
538 2020, 2020.
539
- 540 Liao, H., Chang, W., Yang, Y.: Climatic effects of air pollutants over China: A review, *Advances in*
541 *Atmospheric Sciences*, 32, 115–139, <https://doi.org/10.1007/s00376-014-0013-x>, 2015.
542
- 543 Le, T., Wang, Y., Liu, L., Yang, J., Yung, Y. L., Li, G., Seinfeld, J. H.: Unexpected air pollution with
544 marked emission reductions during the COVID-19 outbreak in China, *Science*, 369, 702–706,
545 <https://doi.org/10.1126/science.abb7431>, 2020.
546
- 547 Le Quéré, C., Jackson, R. B., Jones, M. W., Smith, A. J. P., Abernethy, S., Andrew, R. M., De-Gol,
548 A. J., Willis, D. R., Shan, Y. L., Canadell, J. G., Friedlingstein, P., Felix Creutzig, F., Peters,
549 G., P.: Temporary reduction in daily global CO₂ emissions during the COVID-19 forced
550 confinement, *Nature Climate Change*, 10, 647–653, [https://doi.org/10.1038/s41558-020-0797-](https://doi.org/10.1038/s41558-020-0797-x)
551 x, 2020.
552
- 553 Lelieveld, J., Klingmüller, K., Pozzer, A., Burnett, R. T., Haines, A., Ramanathan, V.: Effects of fossil
554 fuel and total anthropogenic emission removal on public health and climate. *Proceedings of*
555 *the National Academy of Sciences*, 116, 7192–7197, <https://doi.org/10.1073/pnas.1819989116>,
556 2019.
557
- 558 Li, L., Li, Q., Huang, L., Wang, Q., Zhu, A., Xu, J., Liu, Z., Li, H., Shi, L., Li, R., Azari, M., Wang,
559 Y., Zhang, X., Liu, Z., Zhu, Y., Zhang, K., Xue, S., Ooi, M., C., G., Zhang, D., Chan, A.: Air
560 quality changes during the COVID-19 lockdown over the Yangtze River Delta Region: An
561 insight into the impact of human activity pattern changes on air pollution variation. *Science of*
562 *The Total Environment*, 732, 139282. <https://doi.org/10.1016/j.scitotenv.2020.139282>, 2020.
563
- 564 Liu, X., Easter, R. C., Ghan, S. J., Zaveri, R., Rasch, P., Shi, X., Lamarque, J., F., Gettelman, A.,
565 Morrison, H., Vitt, F., Conley, A., Park, S., Neale, R., Hannay, C., Ekman, A. M. L., Hess, P.,
566 Mahowald, N., Collins, W., Iacono, M. J., Bretherton, C. S., Flanner, M. G., Mitchell, D.:



- 567 Toward a minimal representation of aerosols in climate models: description and evaluation in
568 the Community Atmosphere Model CAM5, *Geoscientific Model Development*, 5, 709–739.
569 <https://doi.org/10.5194/gmd-5-709-2012>, 2012.
- 570
- 571 Liu, Y., Hong, Y., Fan, Q., Wang, X., Chan, P., Chen, X., Lai, A., Wang, M., Chen, X.: Source-
572 receptor relationships for PM_{2.5} during typical pollution episodes in the Pearl River Delta city
573 cluster, China, *Science of The Total Environment*, 596, 194–206,
574 <https://doi.org/10.1016/j.scitotenv.2017.03.255>, 2017.
- 575
- 576 Ramanathan, V. C. P. J., Crutzen, P. J., Kiehl, J. T., Rosenfeld, D.: Aerosols, climate, and the
577 hydrological cycle, *science*, 294, 2119–2124, <https://doi.org/10.1126/science.1064034>, 2001.
- 578
- 579 Ren, L., Yang, Y., Wang, H., Zhang, R., Wang, P., Liao, H.: Source attribution of Arctic aerosols and
580 associated Arctic warming trend during 1980–2018, *Atmospheric Chemistry and Physics*, 20,
581 9067–9085, <https://doi.org/10.5194/acp-2020-3,2020>.
- 582
- 583 Sharma, S., Zhang, M., Anshika, Gao, J., Kota, S. H.: Effect of restricted emissions during covid-
584 19 on air quality in india, *Science of The Total Environment*, 728, 138878,
585 <https://doi.org/10.1016/j.scitotenv.2020.138878>, 2020.
- 586
- 587 Smith, C. J., Kramer, R. J., Myhre, G., Alterskjær, K., Collins, W., Sima, A., Boucher, O., Dufresne,
588 J.-L., Nabat, P., Michou, M., Yukimoto, S., Cole, J., Paynter, D., Shiogama, H., O'Connor, F.
589 M., Robertson, E., Wiltshire, A., Andrews, T., Hannay, C., Miller, R., Nazarenko, L., Kirkevåg,
590 A., Olivie, D., Fiedler, S., Lewinschal, A., Mackallah, C., Dix, M., Pincus, R., Forster, P. M.:
591 Effective radiative forcing and adjustments in CMIP6 models, *Atmospheric Chemistry and*
592 *Physics*, 20, 9591–9618, <https://doi.org/10.5194/acp-20-9591-2020>, 2020.
- 593
- 594 Tian, H., Liu, Y., Li, Y., Wu, C., Chen, B., Kraemer, M.U.G., Li, B., Cai, J., Xu, B., Yang, Q., Wang,
595 B., Yang, P., Cui, Y., Song, Y., Zheng, P., Wang, Q., Bjornstad, O.N., Yang, R., Grenfell, B.T.,
596 Pybus, O.G., Dye, C.: An investigation of transmission control measures during the first 50
597 days of the COVID-19 epidemic in China, *Science*, b6105
598 <https://doi.org/10.1126/science.abb6105>, 2020.
- 599
- 600 Vautard, R., Yiou, P., Oldenborgh, G.: Decline of fog, mist and haze in Europe over the past 30 years,
601 *Nature Geoscience*, 2, 115–119, <https://doi.org/10.1038/ngeo414>, 2009.
- 602
- 603 Wang, H., Easter, R. C., Rasch, P. J., Wang, M., Liu, X., Ghan, S. J., Qian, Y., Yoon, J.-H., Ma, P.-
604 L., Vinoj, V.: Sensitivity of remote aerosol distributions to representation of cloud–aerosol
605 interactions in a global climate model, *Geoscientific Model Development*, 6, 765–782,
606 <https://doi.org/10.5194/gmd-6-765-2013>, 2013.
- 607
- 608 Wang, H., Rasch, P. J., Easter, R. C., Singh, B., Zhang, R., Ma, P. L., Qian, Y., Ghan, S. J., Beagley,
609 N.: Using an explicit emission tagging method in global modeling of source-receptor
610 relationships for black carbon in the Arctic: Variations, sources, and transport pathways,



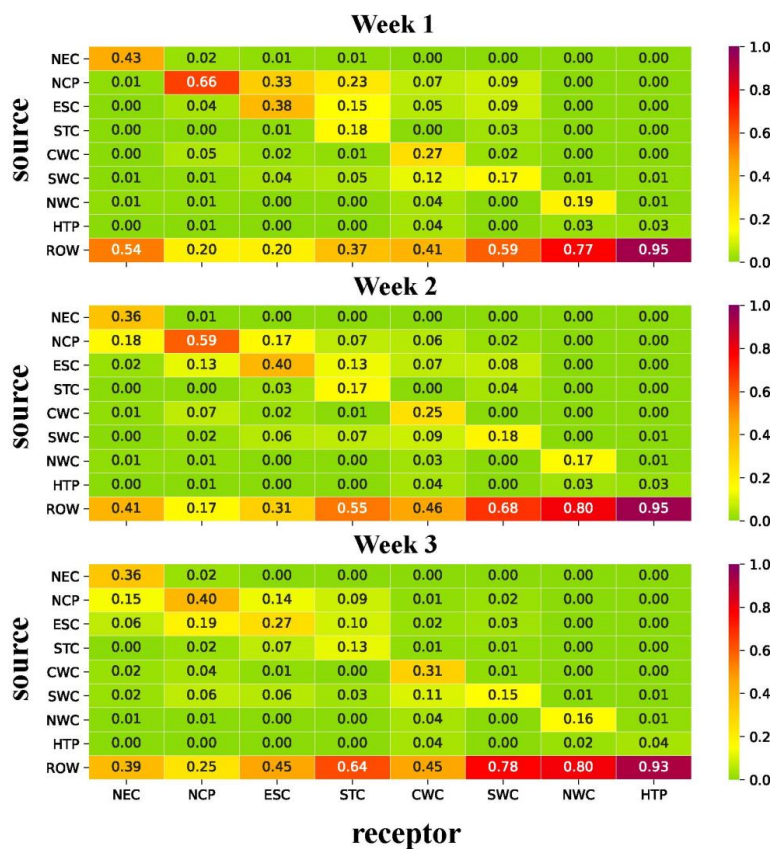
- 611 Journal of Geophysical Research, 119, 12888–12909, <https://doi.org/10.1002/2014JD022297>,
612 2014.
613
- 614 Wang, H., Easter, R. C., Zhang, R., Ma, P., Singh, B., Zhang, K., Ganguly, D., Rasch, P. J., Burrows,
615 S. M., Ghan, S. J., Lou, S., Qian, Y., Yang, Y., Feng, Y., Flanner, M., Leung, L. R., Liu, X.,
616 Shrivastava, M., Sun, J., Tang, Q., Xie, S., Yoon, J.: Aerosols in the E3SM Version 1: New
617 Developments and Their Impacts on Radiative Forcing, *Journal of Advances in Modeling Earth
618 Systems*, 12, 293, <https://doi.org/10.1029/2019MS001851>, 2020.
619
- 620 Wang, P., Chen, K., Zhu, S., Wang, P., Zhang, H.: Severe air pollution events not avoided by reduced
621 anthropogenic activities during COVID-19 outbreak, *Resources Conservation and Recycling*,
622 158, 104814, <https://doi.org/10.1016/j.resconrec.2020.104814>, 2020.
623
- 624 Wang, Q., Huang, R. J., Cao, J., Tie, X., Shen, Z., Zhao, S., Han, Y., Li, G., Li, Z., Ni, H., Zhou, Y.,
625 Wang, M., Chen, Y., Zhou, Y.: Contribution of regional transport to the black carbon aerosol
626 during winter haze period in Beijing, *Atmospheric Environment*, 132, 11–28,
627 <https://doi.org/10.1016/j.atmosenv.2016.02.031>, 2016.
628
- 629 Watson, J. G.: Visibility: Science and regulation. *Journal of the Air and Waste Management
630 Association*, 52, 628–713, <https://doi.org/10.1080/10473289.2002.10470813>, 2002.
631
- 632 Xu, Q., Wang, S., Jiang, J., Bhattarai, N., Li, X., Chang, X., Qiu, X., Zheng, M., Hua, Y., Hao, J.:
633 Nitrate dominates the chemical composition of PM_{2.5} during haze event in Beijing, China, *The
634 Science of the Total Environment*, 689, 1293–1303.
635 <https://doi.org/10.1016/j.scitotenv.2019.06.294>, 2019.
636
- 637 Xue, W. B., Fu, F., Wang, J. N., Tang, G. Q., Lei, Y., Yang, J. T., Wang, Y. S.: Numerical study on
638 the characteristics of regional transport of PM_{2.5} in China, *Journal of Environmental Sciences-
639 China*, 34, 1361–1368, 2014.
640
- 641 Yang, Y., Wang, H., Smith, S. J., Ma, P. L., Rasch, P. J.: Source attribution of black carbon and its
642 direct radiative forcing in China, *Atmospheric Chemistry and Physics*, 17, 4319–4336,
643 <https://doi.org/10.5194/acp-17-4319-2017>, 2017a.
644
- 645 Yang, Y., Wang, H., Smith, S. J., Easter, R., Ma, P. L., Qian, Y., Yu, H., Li, C., Rasch, P. J.: Global
646 source attribution of sulfate concentration and direct and indirect radiative forcing,
647 *Atmospheric Chemistry and Physics*, 17, 8903–8922, [https://doi.org/10.5194/acp-17-8903-
648 2017](https://doi.org/10.5194/acp-17-8903-2017), 2017b.
649
- 650 Yang, Y., Wang, H., Smith, S. J., Zhang, R., Lou, S., Qian, Y., Ma, P.-L., Rasch, P. J.: Recent
651 intensification of winter haze in China linked to foreign emissions and meteorology, *Scientific
652 Reports*, 8, 2107, <https://doi.org/10.1038/s41598-018-20437-7>, 2018a.
653
- 654 Yang, Y., Wang, H., Smith, S. J., Easter, R. C., Rasch, P. J.: Sulfate aerosol in the Arctic: Source



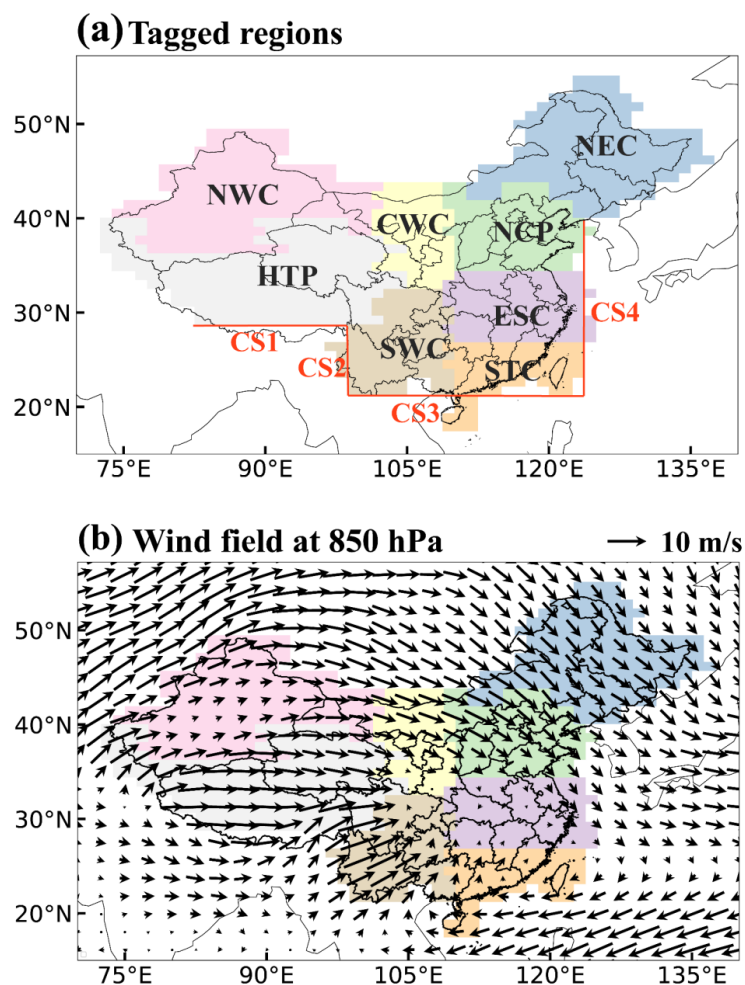
- 655 attribution and radiative forcing, *Journal of Geophysical Research: Atmospheres*, 123, 1899–
656 1918, <https://doi.org/10.1002/2017JD027298>, 2018b.
657
- 658 Yang, Y., Wang, H., Smith, S. J., Zhang, R., Lou, S., Yu, H., Li, C., Rasch, P. J.: Source
659 apportionments of aerosols and their direct radiative forcing and long-term trends over
660 continental United States, *Earth's Future*, 6, 793–808, <https://doi.org/10.1029/2018EF000859>,
661 2018c.
662
- 663 Yang, Y., Smith, S. J., Wang, H., Lou, S., Rasch, P. J.: Impact of anthropogenic emission injection
664 height uncertainty on global sulfur dioxide and aerosol distribution, *Journal of Geophysical
665 Research: Atmospheres*, 124, 4812–4826, <https://doi.org/10.1029/2018JD030001>, 2019a.
666
- 667 Yang, Y., Smith, S. J., Wang, H., Mills, C. M., Rasch, P. J.: Variability, timescales, and nonlinearity
668 in climate responses to black carbon emissions, *Atmospheric Chemistry and Physics*, 19, 2405–
669 2420, <https://doi.org/10.5194/acp-19-2405-2019>, 2019b.
670
- 671 Yang, Y., Lou, S., Wang, H., Wang, P., Liao, H.: Trends and source apportionment of aerosols in
672 Europe during 1980–2018, *Atmospheric Chemistry and Physics*, 20, 2579–2590,
673 <https://doi.org/10.5194/acp-20-2579-2020>, 2020.
674
- 675 Yu, H. B., Remer, L. A., Chin, M., Bian, H. S., Tan, Q., Yuan, T. L., Zhang, Y.: Aerosols from
676 overseas rival domestic emissions over North America, *Science*, 337, 566–569,
677 <https://doi.org/10.1126/science.1217576>, 2012.
678
- 679 Yu, H., Remer, L. A., Chin, M., Bian, H., Kleidman, R. G., Diehl, T.: A satellite-based assessment
680 of transpacific transport of pollution aerosol, *Journal of Geophysical Research*, 113, D14S12,
681 <https://doi.org/10.1029/2007JD009349>, 2008.
682
- 683 Zhang, R., Wang, H., Hegg, D. A., Qian, Y., Doherty, S. J., Dang, C., Ma, P. L., Rasch, P. J., Fu, Q.:
684 Quantifying sources of black carbon in western North America using observationally based
685 analysis and an emission tagging technique in the Community Atmosphere Model,
686 *Atmospheric Chemistry and Physics*, 15, 12,805–12,822, [https://doi.org/10.5194/acpd-15-
687 12957-2015](https://doi.org/10.5194/acpd-15-12957-2015), 2015.
688
- 689 Zheng, B., Tong, D., Li, M., Liu, F., Hong, C., Geng, G., Li, H., Li, X., Peng, L., Qi, J., Yan, L.,
690 Zhang, Y., Zhao, H., Zheng, Y., He, K., Zhang, Q.: Trends in China's anthropogenic emissions
691 since 2010 as the consequence of clean air actions, *Atmospheric Chemistry and Physics*, 18,
692 14095–14111, <https://doi.org/10.5194/acp-18-14095-2018>, 2018.



693 **Table 1.** Fractional contributions of emissions from nine tagged source regions (vertical
 694 axis) to mean PM_{2.5} column burden in eight receptor regions (horizontal axis) during
 695 the three time periods.
 696



697
 698



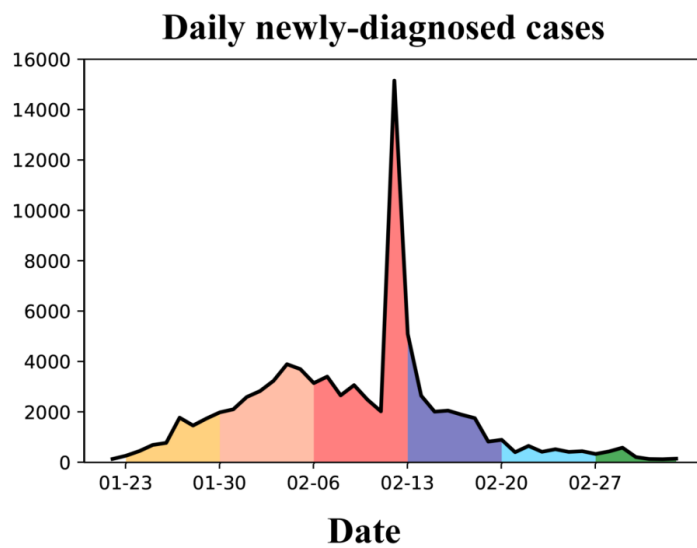
699

700

701 **Figure 1.** (a) Tagged source regions (NEC: Northeastern China, NCP: North China
702 Plain, ESC: Eastern China, STC: Southern China, CWC: Central-West China, SWC:
703 Southwestern China, NWC: Northwestern China, HTP: Himalayas and Tibetan Plateau,
704 ROW: rest of the world) and (b) mean wind field (units: m s^{-1} , vectors) at 850 hPa
705 during the time period of interest. Lines in (a) mark the cross-sections (CS) defined to
706 study the transport of aerosols to and from China.

707

708



709

710

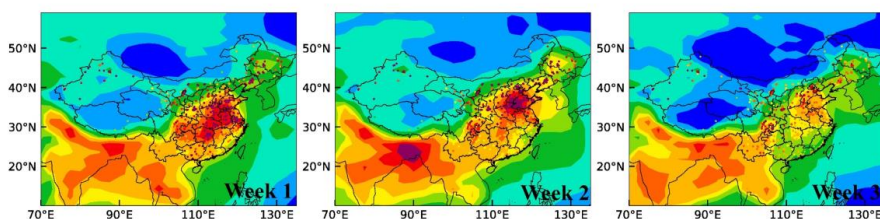
711 **Figure 2.** The number of daily newly-diagnosed cases in China from January 23 to

712 February 27, 2020, during the COVID-19.

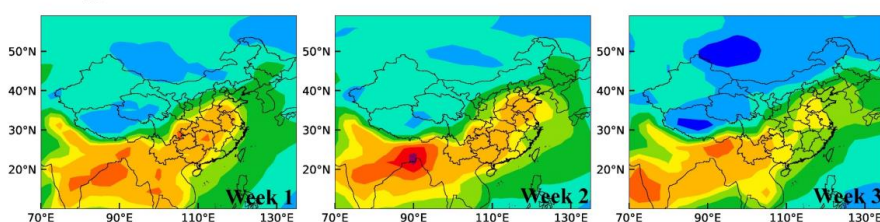
713



(a) $\text{PM}_{2.5}$ surface conc. ($\mu\text{g m}^{-3}$)



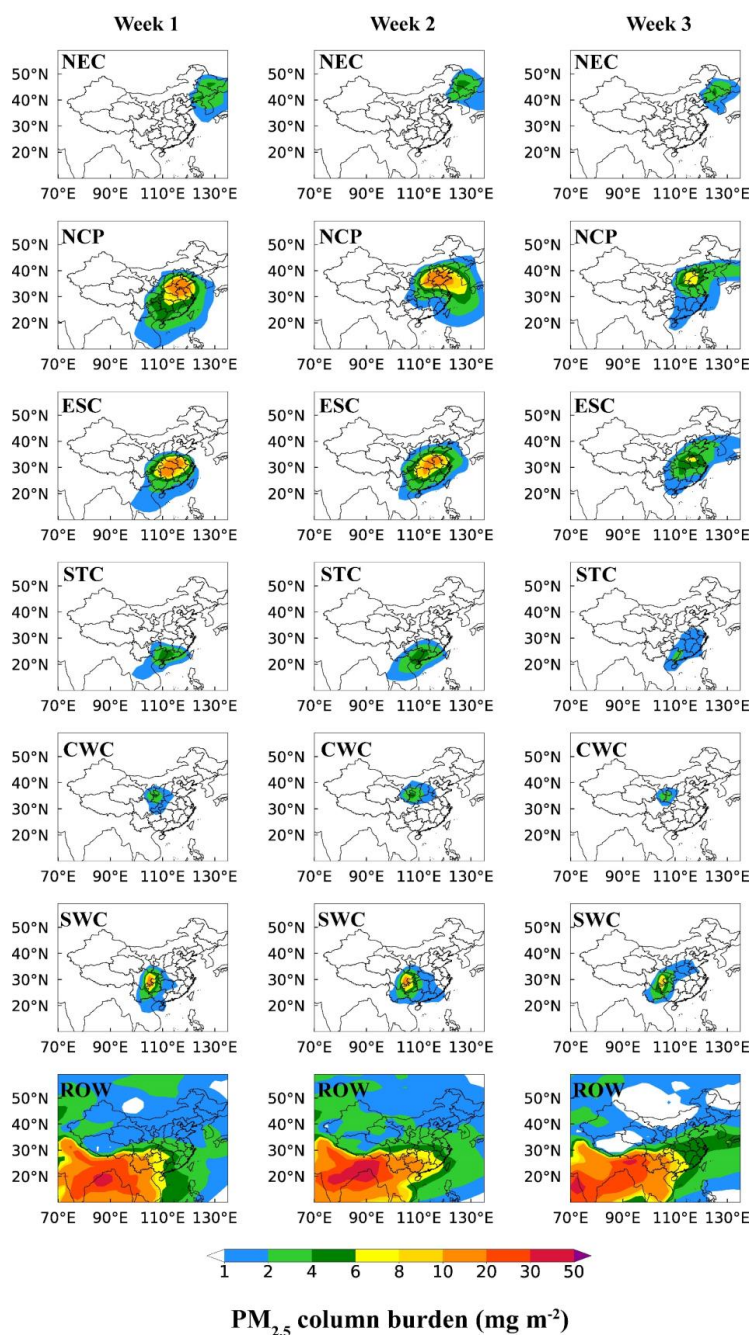
(b) $\text{PM}_{2.5}$ column burden (mg m^{-2})



714

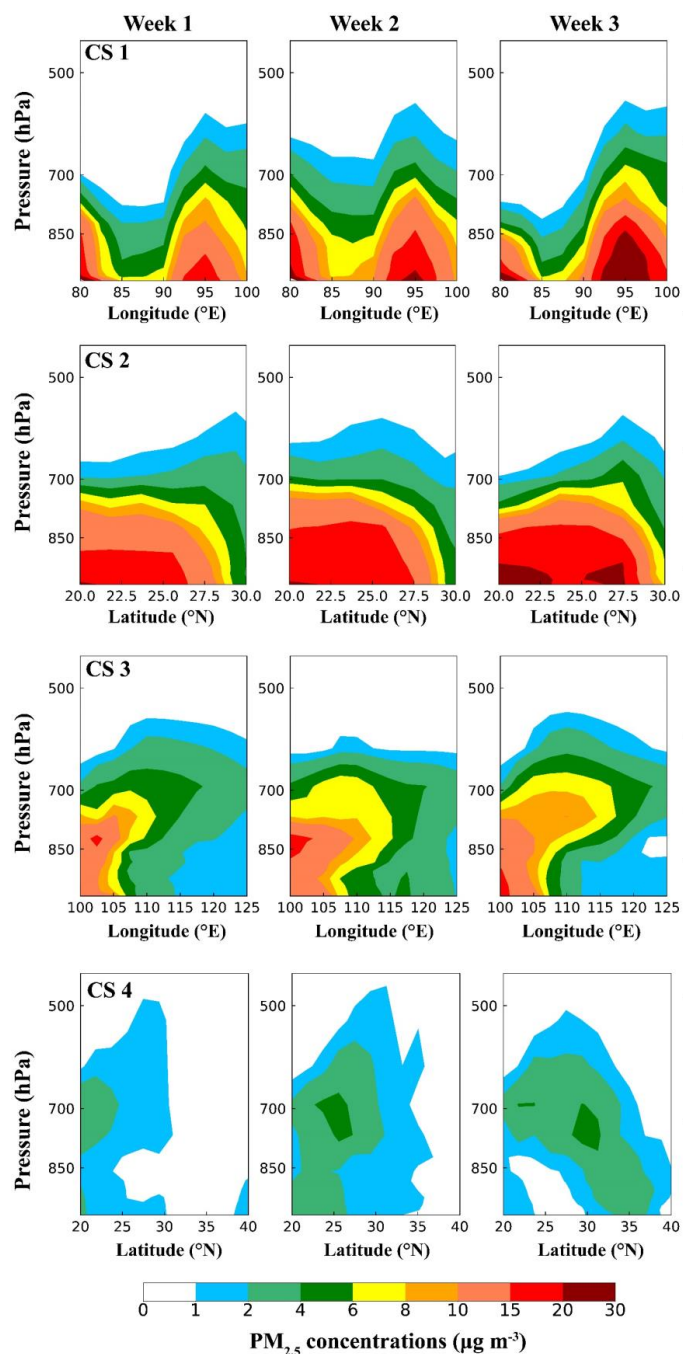
715

716 **Figure 3.** Spatial distribution of (a) the simulated and observed mean near-surface
717 $\text{PM}_{2.5}$ concentrations ($\mu\text{g m}^{-3}$) and (b) $\text{PM}_{2.5}$ column burden (mg m^{-2}) during January
718 30–February 5 (Week 1), February 6–February 12 (Week 2) and February 13–February
719 19 (Week 3).



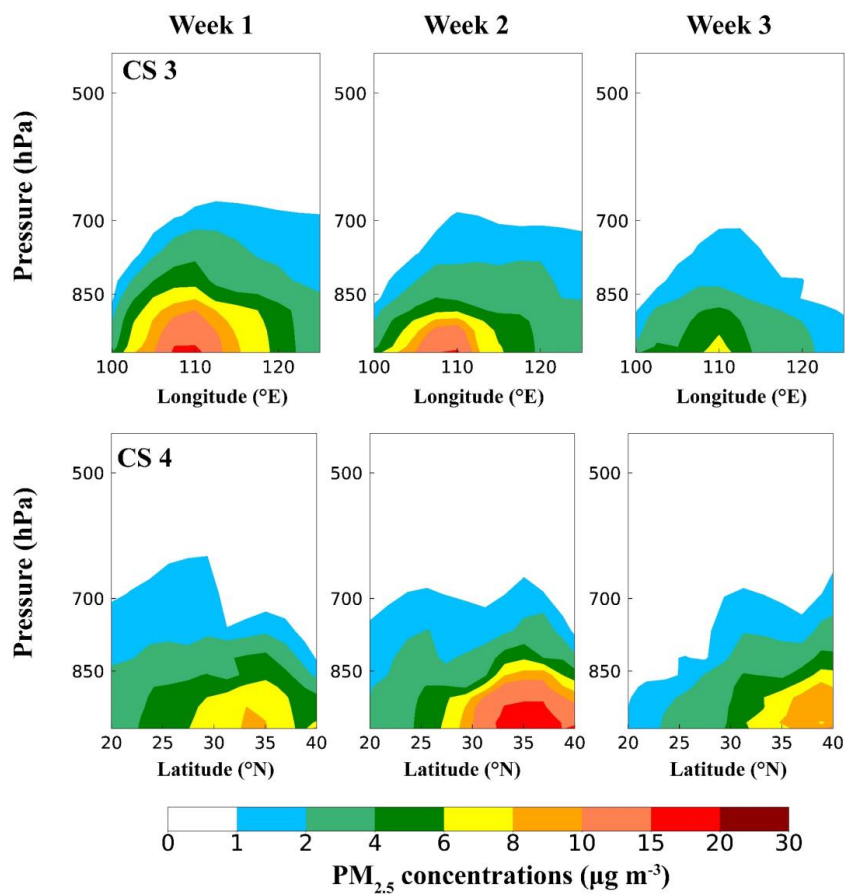
720
721
722
723
724

Figure 4. Spatial distribution of $\text{PM}_{2.5}$ column burden (mg m^{-2}) originating from the six major source regions in China (NEC, NCP, ESC, STC, CWC and SWC) and sources outside China (ROW) during the three time periods.



725

726 **Figure 5.** Vertical distributions of PM_{2.5} concentrations (µg m⁻³), originating from
727 emissions outside China (i.e., ROW sources), across the latitudinal and/or longitudinal
728 extents marked in Fig. 1, respectively, during the three time periods.

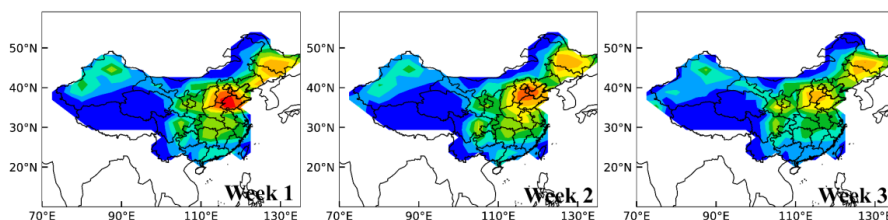


729
730
731
732
733
734
735
736

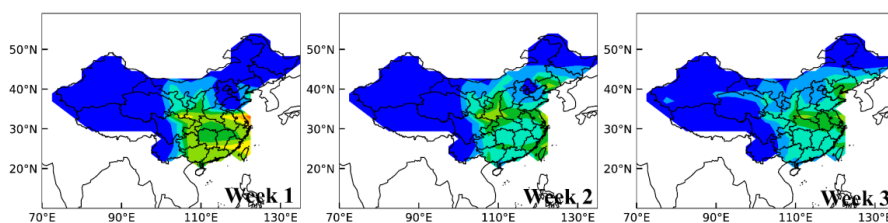
Figure 6. Vertical distributions of $\text{PM}_{2.5}$ concentrations ($\mu\text{g m}^{-3}$), originating from domestic emissions in China, across the latitudinal and/or longitudinal extents marked in Fig.1, respectively, during the three time periods. The values along CS 1 and CS 2 are negligibly small.



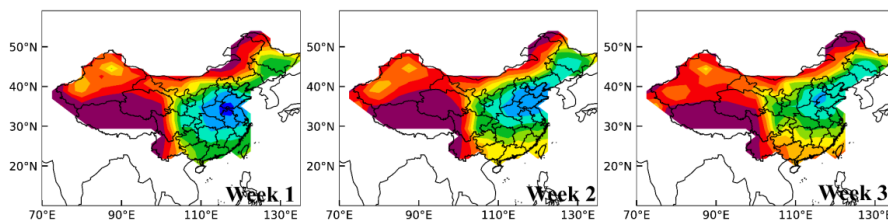
(a) Local contribution



(b) RCN contribution



(c) ROW contribution



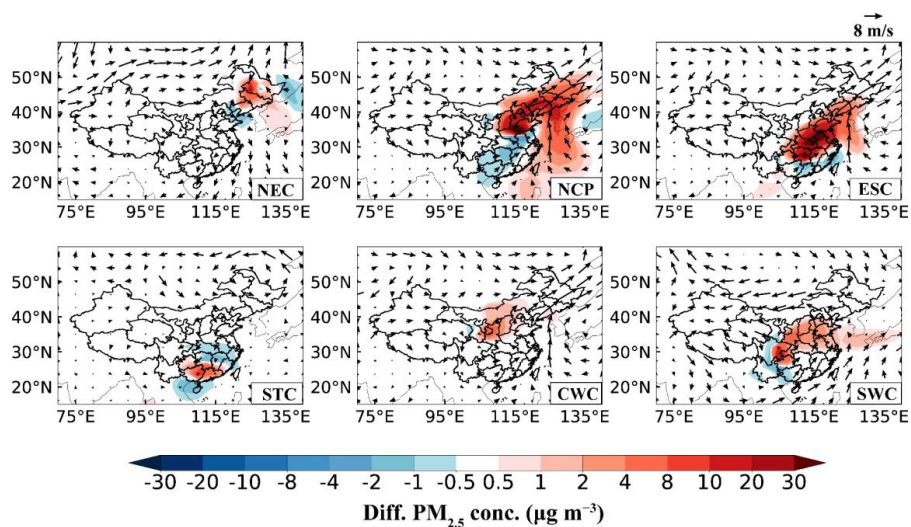
Relative contribution to PM_{2.5} column burden (%)

737

738

739 **Figure 7.** Relative contributions (%) of (a) local emissions, (b) the emissions from the
740 rest of China (RCN) and (c) all sources outside China (rest of the world, ROW) to PM_{2.5}
741 column burden during the three time periods.

742

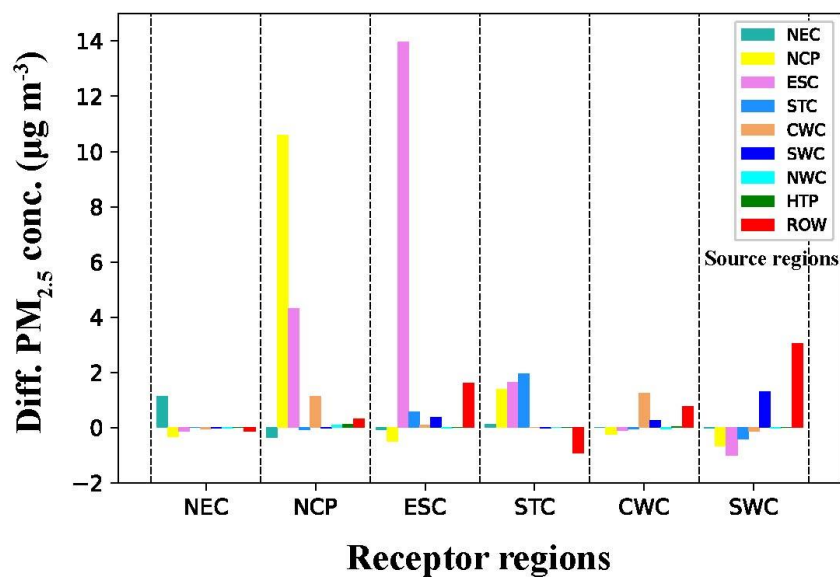


743

744

745 **Figure 8.** Composite differences in winds at 850 hPa (m s^{-1}) and near-surface $\text{PM}_{2.5}$
746 concentrations ($\mu\text{g m}^{-3}$) between polluted and normal days in February 2020. The
747 polluted day is defined as the day with the highest daily $\text{PM}_{2.5}$ concentration in February
748 2020 in each receptor region in China.

749



750

751

752 **Figure 9.** Composite differences in near-surface PM_{2.5} concentrations (µg m⁻³)
753 averaged over receptor regions (marked on the horizontal axis) in China between
754 polluted and normal days in February 2020 originating from individual source regions
755 (corresponding color bars in each column).